Separation and Purification Technology 301 (2022) 122024

Contents lists available at ScienceDirect

Separation and Purification Technology

journal homepage: www.elsevier.com/locate/seppur

Synthesis of defective MOF-801 via an environmentally benign approach for diclofenac removal from water streams

Nicholaus Prasetya [1], Kang Li [*]

Barrer Centre, Department of Chemical Engineering, Imperial College London, Exhibition Road, London SW7 2AZ, United Kingdom

ARTICLE INFO

Keywords:
Defective MOF-801
Diclofenac
Adsorption
Metal–organic frameworks

ABSTRACT

Diclofenac is one of the most popular non-steroidal anti-inflammatory drugs (NSAIDs) which has been widely used worldwide. Despite its popularity, its accumulation in the environment poses danger to the aquatic lives and its removal from the environment is paramount important. Although some conventional adsorbents such as activated carbon can be readily used to address this issue, they usually suffer from low diclofenac adsorption capacity (around 200 mg g^{-1}), resulting in bulky adsorption systems. To overcome this problem, high performance materials such as metal organic frameworks (MOFs) can be employed. Here, we report that we synthesised defective MOF-801 for enhanced diclofenac adsorption via a simple and environmentally benign approach. Differing from a conventional MOF synthesis that usually requires the use of organic solvents at high temperature, the defective MOF-801 could be synthesised at room temperature and by changing the reaction medium from dimethylformamide to water. In addition, we have also successfully shown in this study that the defect concentration in MOF-801 can be rationally tuned by adjusting the modulator concentration (formic acid) in the synthesis solution. The resulting defective MOF-801 can then be used for environmental remediation, which we have shown here by employing them as an adsorbent for diclofenac removal from water streams. The enhanced adsorption of defective MOF-801 in comparison to its non-defective counterpart is due to the pore enlargement of the defective MOF-801 which provides a better pathway to access the adsorption sites. The maximum diclofenac adsorption capacity in a highly defective MOF-801 can reach as high as 680 mg g^{-1}, which is almost 4 times higher than its non-defective counterpart. This study then opens possibilities to engineer the MOF particles for environmental remediation.

1. Introduction

Diclofenac is one of the most popular non-steroidal anti-inflammatory drugs that has been used worldwide. Despite its popularity, prevention of its immediate release to the environment is crucial since its accumulation can be harmful to the surrounding ecosystem. For instance, the presence of excessive diclofenac in the environment could poison the aquatic lives [1]. A number of adsorbents such as biochar [2], activated carbon [3–5],organoclays [6], zeolite [7] and graphene oxide (GO) [8,9] have then been investigated as the potential materials to tackle the issue. However, the major problem of these materials lies in their low diclofenac adsorption capacity (i.e. 100–200 mg g^{-1}). Therefore, it is imperative to functionalise the adsorbents or to fabricate high performance materials to increase the diclofenac adsorption capacity [3,10–15].

During the last two decades, there has been a growing interest in the development of metal–organic frameworks (MOFs) as a promising class of porous materials that can be applied to address various environmental issues. Among the numerous types of MOFs, zirconium-based MOFs have demonstrated excellent performances for water-based applications, particularly in maintaining their robust structures. This is because they are built by strong coordination bonding between the zirconium ion and the ligands. Therefore, they have been widely investigated for various purposes such as fluoride removal and desalination [16–18]. In addition, the efficacy of zirconium-based MOFs to eliminate various pharmaceutical products, including diclofenac, from water streams have also been studied recently [19].

MOF-801 is constructed by $Zr_6O_4(OH)_4$ and fumarate as the metal

* Corresponding author.
E-mail address: kang.li@imperial.ac.uk (K. Li).
[1] Current address: Institute of Functional Interface, Karlsruhe Institute of Technology, Hermann-von-Helmholtz-Platz 1, 76344 Eggenstein-Leopoldshafen, Germany.

https://doi.org/10.1016/j.seppur.2022.122024
Received 15 June 2022; Received in revised form 20 August 2022; Accepted 24 August 2022
Available online 27 August 2022

cluster and ligand, respectively. It has a similar topology compared with UiO-66 and was firstly reported in 2012 where both $ZrCl_4$ and fumaric acid were reacted in a solvothermal condition with the presence of formic acid as the modulator [20]. Since then, the research interest in MOF-801 has significantly increased. This is particularly driven by its promising application as a water harvester which utilises the surrounding humidity to produce fresh water [21] and as an adsorbent for cooling system [22].

Because of the excellence of the MOF-801 framework stability in an aqueous environment, MOF-801 may also have its potential as an adsorbent for pollutants removal such as diclofenac. However, its adsorption capacity may not be high enough because of its similar structure with UiO-66, that has relatively low diclofenac uptake (around 100–200 mg g^{-1}) [23,24]. Therefore, functionalisation of such MOFs is sometimes necessary to significantly improve its diclofenac uptake [25], which could render the whole MOF production more complex.

To address the issue, we hypothesise that the diclofenac uptake of MOF-801 can actually be rationally improved by defect engineering. Introducing defects have been widely studied in various MOFs, such as in MOF-808 [26], MOF-74 [27], UiO-66 [28,29] and MOF-801 [22,30,31] and can be considered as one of the effective strategies to broaden MOFs' applicability [29,32]. In our case, this approach could be beneficial since it can enlarge the pore opening of the MOFs so the diclofenac molecule can easily access the adsorptive sites in the pores of the defective MOFs. This approach is also based on the fact that high diclofenac uptake could be achieved by employing MOFs with large pore aperture and surface area [19].

In this study, we then propose a new strategy to create defects in MOF-801 through a simple and environmentally benign approach. Differing from the conventional synthesis of MOF-801 that requires harmful DMF as the solvent at high temperature, the defective MOF-801 could be synthesised using water as the solvent at room temperature. The concentration of defects in MOF-801 could also be fine-tuned by adjusting the amount of formic acid used during the synthesis. In this study, both the non-defective and defective MOF-801 were then fully characterised and their environmental remediation potential, which in this study is exemplified by studying its diclofenac removal capability, were also studied comprehensively, including isotherm, thermodynamic and the adsorption kinetics to demonstrate the superiority of introducing defects in MOF-801 to enhance its capability in removal of diclofenac from water streams.

2. Materials and methodology

2.1. Chemicals

Zirconia tetrachloride ($ZrCl_4$), fumaric acid and diclofenac sodium salt were purchased from Merck, United Kingdom. Dimethylformamide (DMF) and formic acid were purchased from VWR, United Kingdom.

2.2. Synthesis of MOF-801 nanoparticles

There are two different methods used in this study to synthesise MOF-801 nanoparticlesTable 1.. The first method used dimethylformamide (DMF) as the solvent to synthesise the MOF-801 that contains the least defects. The synthesis condition was adapted from the previous report on the synthesis of Zr-fumarate [20]. In a typical synthesis, 120 mg of $ZrCl_4$ and 180 mg of fumaric acid were dissolved in 20 mL DMF. To this solution, 100 equivalent of formic acid was added as a modulator. The solution was then transferred into a Teflon-lined autoclave and the solvothermal reaction took place in a convective oven at 120 °C for 24 h. Once the reaction finished, the product was collected by filtration and then washed with DMF and methanol. Afterwards, the product was immersed in methanol for 3 days to remove the DMF from the MOF pores. During this period, the methanol was exchanged with a fresh methanol twice a day. The MOF-801 was then dried at 100 °C before being used for adsorption studies.

Meanwhile, the second method was employed to produce MOF-801 with more defects. In this case, water was used instead of DMF as the solvent. In brief, 350 mg of $ZrCl_4$ and 160 mg of fumaric acid were used as the starting materials. They were dissolved in 8 mL of deionised water and varying amount of formic acid. Afterwards the solution was sonicated for 1 h and left at room temperature for 24 h. The products were collected by centrifugation (12000 RPM) and washed with DI water and ethanol. The defective-MOF-801 were then dried at 100 °C before being used for adsorption studies.

For the sake of naming convenience, throughout this research, the sample that was synthesised using the first method is named MOF-801 to indicate that it contains the least defects. Meanwhile, the samples from the second method are named d-MOF-801(n). The 'd' indicates the samples contain more defects than the MOF-801 synthesised through the first method and the 'n' indicates the equivalent amount of formic acid added to the synthesis condition as described above. Therefore, for example, d-MOF-801(35) means that the defective-MOF-801 was synthesised using 350 mg of ZrCl4, 160 mg of fumaric acid, 8 mL of DI water and 35 equivalent of formic acid relative to the $ZrCl_4$. A typical synthesis condition for both d-MOF-801(n) and MOF-801 is then given in 1.

2.3. Characterisations

2.3.1. Powder X-Ray diffraction (PXRD)

Powder X-Ray Diffraction (PXRD) technique was employed to characterise the crystallinity of the samples. The nanopowder of both d-MOF-801(n) and MOF-801 was spread over the sample holder. PANanlytical XRD was then used as to obtain the PXRD spectra of the samples. The voltage and the current of the instrument were set at 40 kV and 40 mA, respectively, and the measurement took place at 2θ between 5 and 40°.

2.3.2. Fourier transformed infrared (FTIR)

Fourier Transformed Infrared (FTIR) spectra were collected using FTIR Cary Spectrometer to obtain the chemical bonding information in the samples. The measurement took place between the wavenumber 4000–500 cm^{-1} and the sampling technique used in this study is attenuated total reflectance (ATR).

2.3.3. ^1H Nuclear magnetic resonance (NMR)

Nuclear magnetic resonance (NMR) was employed to obtain the

Table 1
Synthesis conditions of both d-MOF-801(n) and MOF-801 used in this study.

MOF	Mass of $ZrCl_4$ (mg)	Mass of fumaric acid (mg)	Solvent	Solvent volume (mL)	Amount of formic acid (mL)	Synthesis method
d-MOF-801 (35)	350	160	Water	8	2	Ultrasonication followed by overnight staying at room temperature
d-MOF-801 (50)	350	160	Water	8	2.8	
d-MOF-801 (70)	350	160	Water	8	4	
MOF-801	120	180	DMF	20	2	Solvothermal for 24 h at 120 °C

information on the ratio between formate and fumarate in the samples. This information can then be used to approximate the extent of defects in the samples. About 1–2 mg of the samples were firstly digested in 1 mL of 4% NaOD/D_2O solution. The digested samples were then filtered through cotton to obtain a clear solution. The NMR spectra of the solution were then collected by using Jeol 400 MHz spectrometer.

2.3.4. Thermogravimetric analysis (TGA)

The thermal stability profile of the samples was evaluated by employing thermogravimetry analysis (TGA) technique. The TGA instrument from Netzsch was also equipped with mass spectrometer to monitor the gas phase that comes out as the temperature in the sample chamber is ramped up. Around 2–4 mg of samples were used to obtain the TGA profile of both d-MOF-801(n) and MOF-801.

2.3.5. Nitrogen physisorption

Specific surface area of the materials was measured at 77 K using Quantachrome iQ3 instrument by using nitrogen as the adsorbate. The sample mass used for this characterization is between 50 and 60 mg. Before the measurement took place, all the samples were degassed under vacuum using the *in-situ* degassing instrument of the instrument. The degassing temperature was set at 110 °C and the degassing took place for at least 15 h.

2.3.6. Scanning electron microscopy (SEM)

The micrographs of the gold-coated samples were obtained by using scanning electron microscope (SEM) LEO Gemini 1525 FEGSEM. The accelerating voltage and working distance were set to be 5 kV and around 6 mm, respectively.

2.3.7. UV–Vis spectroscopy

During the diclofenac adsorption studies, the diclofenac concentration was determined by taking the UV–Vis absorbance value at 276 nm. The absorbance of the samples was collected by using Thermo Fisher Scientific Nanodrop UV–Vis spectrophotometer. Around 10 μL of samples were used to obtain the UV–Vis spectra.

2.4. Diclofenac adsorption study

The diclofenac adsorption study was conducted following the procedure in our previous study [19]. The study of diclofenac adsorption isotherm was carried out by suspending 1 mg of MOF-801 or d-MOF-801 (n) in a 2 mL diclofenac solution with various concentrations. The suspensions were then sonicated, put in a roller miller and left for 24 h to achieve equilibrium. Afterwards, the suspension was filtered using a 0.22 μm syringe filter (Sartorius, cellulose acetate) and the UV–Vis absorbance of the filtrate was measured.

To study the adsorption kinetic of the diclofenac, 5 mg of the MOF-801 or d-MOF-801(n) was dispersed in 10 mL of 500 mg L^{-1} diclofenac solution and sonicated to obtain a homogeneous suspension. The concentration of the diclofenac in the suspension was then monitored at a certain period of time (5, 10, 20, 40, 60, 120, 240 and 360 min). This was accomplished by monitoring the UV–Vis absorbance of the filtrate that was collected by taking out around 1 mL of the suspension using a syringe which was followed by filtering the suspension using a 0.22 μm syringe filter (Sartorius, cellulose acetate). The temperature during the experiment were 298 K.

Meanwhile, only two MOFs, namely MOF-801 and d-MOF-801(35), were involved to study the effect of temperature, pH and the presence of both cation and anion species on the diclofenac adsorption capacity since they represent the most contrasting features. In this case, about 1 mg of MOF was used and suspended in a glass vial containing 2 mL of 500 mg L^{-1} diclofenac solution. To study the effect of the temperature, the glass vial was either placed in controlled temperature room or inside an oil bath during the adsorption process. The effect of pH was studied by carefully adjusting the pH of the suspension using either 0.1 M HCl or 0.1 M NaOH. Lastly, the effect of the presence of various salts on the adsorption process was also evaluated by adding the natrium or chloride salt into the solution. The concentration of the salts is adjusted to be 1 mmol L^{-1} for NaCl, $NaNO_3$ and KCl and 0.5 mmol L^{-1} for Na_2SO_4, Na_2CO_3, $MgCl_2$ and Mg_2SO_4.

Regeneration study was caried out by washing the d-MOF-801(35) with a mixture of methanol and acetic acid (9:1 v/v) overnight. Afterwards the regenerated d-MOF-801(35) was collected and dried at 100 °C before undergoing the next cycle of diclofenac adsorption test.

3. Results and discussions

3.1. MOF-801 and d-MOF-801(n) nanoparticles characterisation

As described in the previous section, two methods were used to synthesise the MOF-801: using either DMF or water as the solvent. The summary of both methods and the expected nanomaterials is then given in Fig. 1. We hypothesise that MOF-801 that is produced by aqueous synthesis method contains more defects than the one that is produced using solvothermal method. In respect to this, it should also be noted that our attempt to produce a perfect MOF-801 using a solvothermal method was unsuccessful despite our numerous trials to change the synthesis conditions. Based on the ^1H NMR spectrum of the digested MOF-801 (Figure S4), it can be seen that the formate peak does still exist and thus indicating the presence of little defects in the MOF-801 structure.

However, it can also be observed from Figures S1-S4 and Table S1, that the presence of defects in MOF-801 is very minimal in comparison to the d-MOF-801(n). In this case, the defect concentration in MOF-801 framework can be indicated by the presence of formate in the framework. It can then be seen that the presence of formate in MOF-801 is found to be around 8%. This is in a stark contrast with d-MOF-801(n). This value in both d-MOF-801(50) and d-MOF-801(35) could reach around 30%. Meanwhile, this value is found to be lower in d-MOF-801 (70), where the percentage is found to be around 25%. This then also shows that the defects concentration could be rationally tuned by adjusting the amount of formic acid used during the aqueous synthesis of d-MOF-801(n). The higher the amount of formic acid used, a least defective d-MOF-801 could be obtained. Meanwhile, it does also seem that further lowering the amount of formic acid during the synthesis does not lead to produce a more defective d-MOF-801. As can be seen from the digested spectrum of d-MOF-801(n), the trend of formate/fumarate ratio in d-MOF-801(n) is rather plateauing. This is probably because MOF-801 could not retain its framework where more defects are introduced within its framework. Meanwhile, our attempt to produce defective MOF-801 using water as the solvent with lesser defective sites was also unsuccessful since increasing the amount of formic acid in the synthesis condition beyond 70 equivalents resulted in a relatively stable solution and no products could be obtained. This also indicates that a modulator window exists to obtain a crystalline d-MOF-801(n). On one hand, the amount of formic acid should not be too low to maintain the robustness of the framework. On the other hand, it should not also be too high that could eventually prevent the crystallisation process to take place.

Various techniques were then used to characterise both the MOF-801 and d-MOF-801(n). Firstly, powder X-Ray diffraction (PXRD) was used to evaluate the crystallinity of the samples and the result is presented in Fig. 2(A). It can be seen from the result that both MOF-801 and d-MOF-801 have identical PXRD spectra that perfectly match with the calculated pattern of MOF-801. This shows that regardless of the presence of defects in the structure, all of the samples crystallise as MOF-801. However, it can also be observed that the relative intensity of the PXRD spectra of d-MOF-801(n) is lower compared with the MOF-801. This is more pronounced with d-MOF-801(35), which was produced using the least amount of formic acid. This indicates that the d-MOF-801 (n) are less crystalline than its MOF-801 counterpart. In addition, this

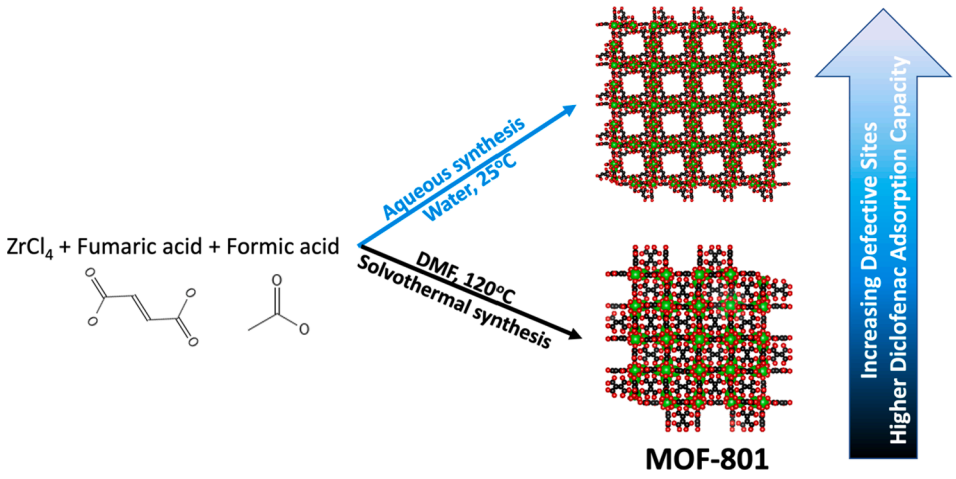

Fig. 1. Strategy to synthesise defective MOF-801 with enhanced diclofenac adsorption.

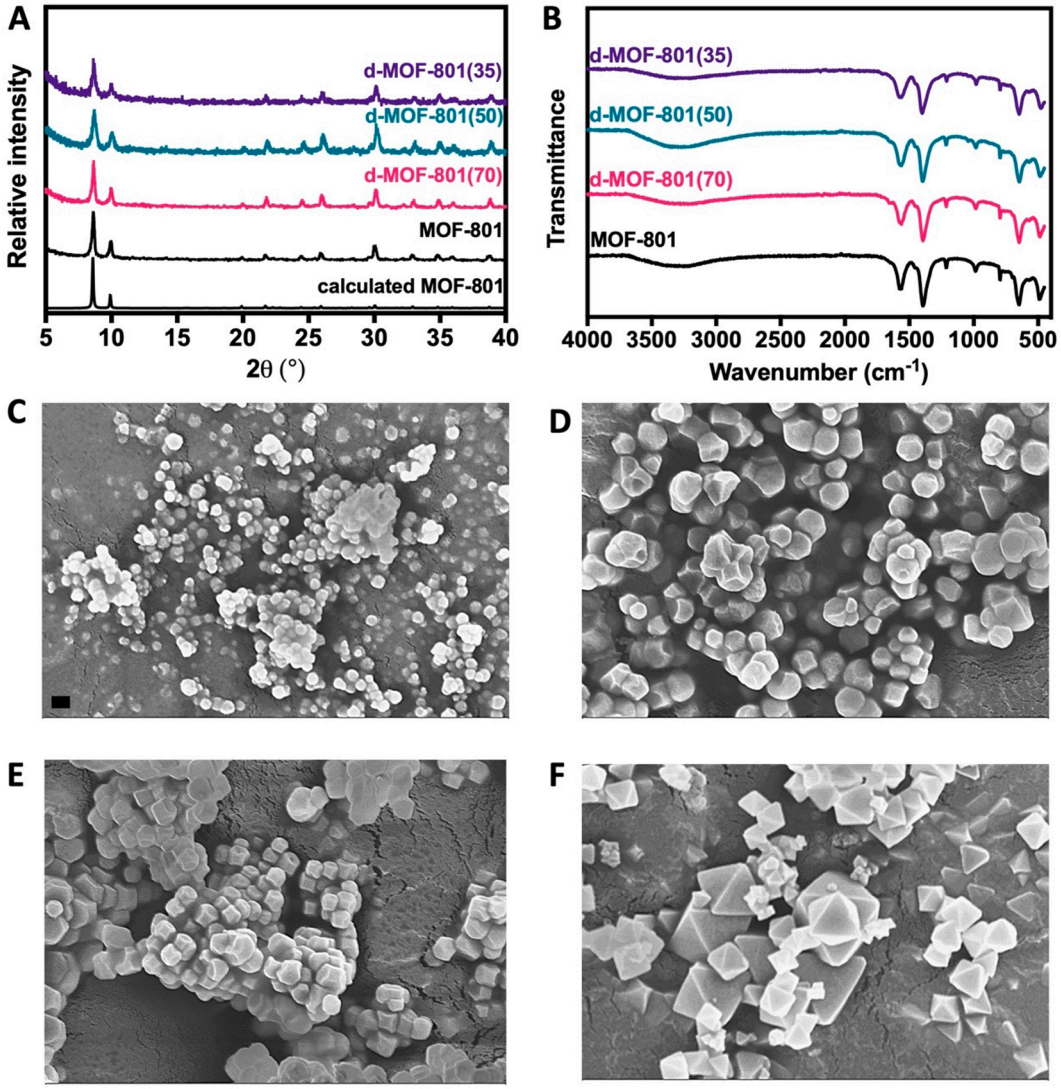

Fig. 2. PXRD pattern (A) and FTIR spectra (B) of MOF-801 and d-MOF-801(n) and SEM pictures of d-MOF-801(35) (C), d-MOF-801(50) (D), d-MOF-801(70) (E) and MOF-801 (F). The scale bar for all SEM figures is 200 nm and given in (C).

also shows that, among the d-MOF-801(n), the higher the formic acid used during the synthesis condition, the higher the crystallinity of the product. This is also in accordance with the first report on Zr-fumarate MOF where higher modulator concentration produces MOF with better crystallinity [20].

Fourier transformed infrared spectroscopy (FTIR) was also employed to elucidate the fingerprint of both the MOF-801 and d-MOF-801(n) and the resultant spectra is presented in Fig. 2(B). From the result, it can be seen that the spectra of both MOF-801 and d-MOF-801(n) resembles each other and there is no significance difference between the two samples. This is probably because all samples still contain both fumaric and formic acid in their structure and thus do not yield any difference in their chemical fingerprint. From the spectra, it can be seen that the characteristic peaks at around 1390 cm^{-1} and 1550 cm^{-1} appear in all samples which are correlated with the carboxylate bonding from the ligand [33]. In addition, peaks at around 1200 cm^{-1} and can also be observed which can be associated with the carboxylic acid group from the fumaric acid.

The micrographs of both d-MOF-801(n) and MOF-801 are given in Fig. 2(C)–(F). From the figure, it can be seen that MOF-801 were formed in two different shapes, where a solvothermal method produces a perfect and well-defined octahedral shape (Fig. 2F). This is also in accordance with other findings when the MOF-801 was synthesised using DMF as the solvent [20]. Meanwhile, such a well-defined feature cannot be clearly observed for d-MOF-801(n), in particular in d-MOF-801(35). As can be seen in Fig. 2(C), d-MOF-801(35) crystallises rather as a sphere with particle size less than 200 nm. In addition, the particles are also heavily agglomerated. This is also in accordance with previous investigations showing that water-based synthesis of MOF-801 results in a spherical particles rather than an octahedral one [34]. Meanwhile, when the amount of modulator in the synthesis medium is increased, d-MOF-801(n) particles with bigger particle size could be obtained (Fig. 2(D) and (E)). This then also highlights another advantage in the synthesis of d-MOF-801(n), namely the possibility to engineer the particle size. In addition, the d-MOF-801(50) and d-MOF-801(70) particles also appear to be less-agglomerated and have started to show a more well-defined shape, albeit still less well-defined when compared to the MOF-801 that was synthesised using DMF as the solvent.

The different particle shape obtained when MOF-801 was synthesised in water and DMF could then be associated with the presence of defective sites in the MOF. In an ideal condition, when the defective sites are minimal, as in the case of MOF-801, a well-defined octahedral MOF-801 with particle size up to around 500 nm could be obtained. In this case, the formate could effectively compete with the fumarate to coordinate with the metal cluster to slow down the reaction. As a result, the self-repair mechanism of the MOF could take place [35].

Meanwhile, a different situation might be encountered in the synthesis condition of d-MOF-801(n). In this case, the formate could not compete with the fumarate as effective as in the case of MOF-801 because the relatively fast nucleation process in the synthesis of d-MOF-801(n). This might then be associated with the use of ultrasonication process. In addition to aiding the dissolution process of the starting components in water, such a process could also fasten the nucleation and crystallisation process of d-MOF-801(n), which could be attributed to the generation of cavitation bubbles. This is also confirmed by our observation, where all the synthesis medium appeared to be very cloudy after 1 h of ultrasonication and thus indicating a fast reaction time. This could then impact the particle size and shape of d-MOF-801(n). As can be seen from the SEM images, d-MOF-801(n) particles are in general smaller and less well-defined than MOF-801. The fast nucleation rate might cause this phenomenon since there is no sufficient time for the d-MOF-801(n) to grow bigger. In addition, this could also affect the particle shape of d-MOF-801(n) particles, particularly d-MOF-801(35), which appear to be more spherical. This might be caused by the tendency of d-MOF-801(n) to minimise the free energy by lowering the surface contribution. Moreover, faster reaction time also produces a more defective MOF. This is because such a fast reaction time hinders the self-repair mechanism to occur. However, as in the case of MOF-801, the presence of formic acid in the synthesis medium could slow down the reaction since it is going to compete with the fumarate to coordinate with the metal cluster, although not as effective as in the case of MOF-801. Therefore, the most prominent effect was observed in d-MOF-801(70) since it had the highest formic acid concentration in the synthesis medium. As a result, self-repair process is much more favourable to take place in the synthesis medium of d-MOF-801(70) rather than in d-MOF-801(35) and d-MOF-801(50) and thus a crystal with less defective site could be obtained. In addition, this condition also delays the nucleation rate in the synthesis medium of d-MOF-801(70) and thus also resulting in a bigger and more well-defined particle than d-MOF-801(35) and d-MOF-801(50). This explanation is also confirmed from the PXRD pattern as shown in Fig. 2(A), showing that higher modulator in d-MOF-801(n) synthesis results in a sharper XRD pattern, indicating better particle crystallinity and bigger particle size.

The thermal stability profile for all samples is given **in** Fig. 3(A). From the results, it can be seen that both MOF-801 and d-MOF-801(n) display two different stability trends. First, both MOF-801 and d-MOF-801(n), lose water when they are heated until 100 °C, as also confirmed by the appearance of a peak at $m/z = 18$ in the mass spectrum as can be seen in Fig. 3(B). Afterwards, both samples go in a different direction. MOF-801 has a more stabilised trend when heated up to 350 °C before the first step of the ligand decomposition occurs. However, the same trend is not observed in the d-MOF-801(n). As can be seen, all d-MOF-801(n) still experience a mass loss until they reach 350 °C where a more pronounce declining mass loss occurs. This indicates that the d-MOF-801(n) has poorer thermal stability than MOF-801, which also corroborates the previous observation in UiO-66 [36]. This continuous mass decline of the d-MOF-801(n) after the removal of surface water can then be associated to the decomposition of formate ligand. As can also be seen from the mass spectra, a slight hump at $m/z = 18$ can also be observed during this phase which can be associated to the release of H_2O from the decomposition of hydrogen group in C-H bonds in formate ligand. The absence of such a continuous mass loss trend within this temperature range in MOF-801 then also indicates the absence or negligible presence of formate in MOF-801. Afterwards, the mass loss trajectory between d-MOF-801(n) and MOF-801 are quite similar where they experience a sharp declining trend where decomposition of fumarate ligand occurs. However, it can be seen that the declining trend in d-MOF-801(n) starts slightly earlier than in MOF-801. This might indicate the more labile framework structure in d-MOF-801(n) because of the presence of defects. Afterwards both MOF-801 and d-MOF-801(n) experience the second step of ligand decomposition that starts at around 600 °C. This step might be attributed to the removal of the remaining carbonate ions that are still strongly coordinated with the Zr^{4+} ions [37,20]. This is also confirmed from the mass spectra that only shows the peak at $m/z = 44$ which corresponds to the release of CO_2.

The porosity of both MOF-801 and d-MOF-801(n) was then evaluated by analysing their surface area through nitrogen physisorption at 77 K. The results for this study are presented in Table 2 and Fig. 4(A). As can be seen, in general, the nitrogen uptake of d-MOF-801(n) is higher compared to the MOF-801. In accordance with this trend, the specific surface area of d-MOF-801(35), d-MOF-801(50), d-MOF-801(70) and MOF-801 are found to be around 1070, 925, 725 and 811 $m^2\ g^{-1}$, respectively. This trend has also been previously observed in other defective MOFs such as UiO-66 where an introduction of defects into the pristine framework results in an increase in the nitrogen uptake during the physisorption. In this case, the defective MOFs have higher porosity than its pristine structure and thus also have higher specific surface area [29,38,36]. In addition to higher specific surface area, further analysis on the pore size distribution has also shown that, in general, d-MOF-801(n) has bigger pore width and volume than its MOF-801 counterpart. As can be seen from Fig. 4(B), the pore size distribution in MOF-801 is dominated within the region of 0.5 and 0.8 nm, in accordance with what

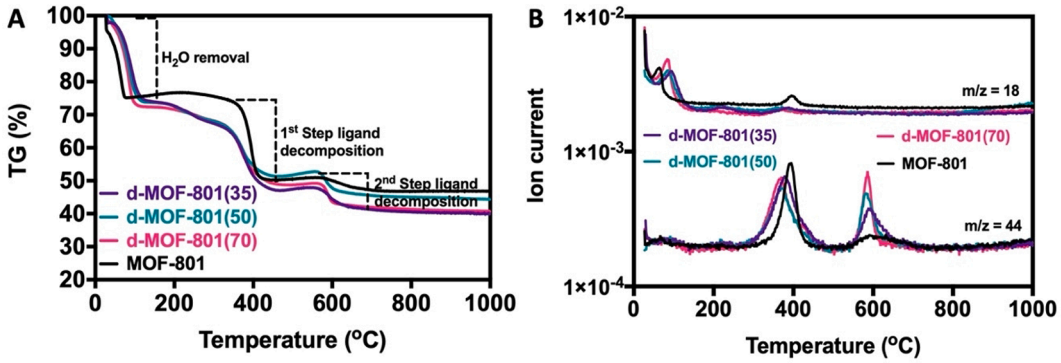

Fig. 3. Thermogravimetric analysis (A) and their corresponding ion current at $m/z = 18$ and $m/z = 44$ (B) of MOF-801 and d-MOF-801(n).

Table 2
Physical properties of both d-MOF-801(n) and MOF-801 obtained from the nitrogen sorption measurement.

MOF	Surface area (m^2 g^{-1})	Pore width (nm)	Pore volume (cm^3 g^{-1})
d-MOF-801 (35)	1070	1.126	0.37
d-MOF-801 (50)	925	1.126	0.32
d-MOF-801 (70)	725	0.6	0.25
MOF-801	811	0.524	0.28

have been previously reported [20,34]. This pore size corresponds to the tetrahedral and octahedral cages, respectively, in MOF-801 [22]. Meanwhile, in d-MOF-801(n), the region at around 0.5 nm starts to disappear and is slightly shifted towards higher value (around 0.6 nm) with the decrease of the concentration of formic acid in the synthesis solution of d-MOF-801(n). This is then accompanied by the increasing domination in the pore size opening region of around 1.2 nm and the decreasing trend in the 0.8 nm pore size region. Therefore, it can also be seen that in the d-MOF-801(35) with the highest defects, the pore size at around 0.8 nm almost entirely disappears and is replaced by two dominant pore regions: 0.6 nm and 1.2 nm. This then clearly indicates that the presence of defects can enlarge the pore opening in the d-MOF-801(n).

However, it should be noted that MOF-801, which was synthesised in this study, also displays a pore opening around 1.2 nm. As has been previously stated, this can be explained by the presence of a small number of defects in the MOF-801. As also corroborated by the ^{1}H NMR spectrum of MOF-801, there is still a minimal presence of formate in MOF-801. They can then contribute in constructing a tiny defective site inside MOF-801 and thus enlarging the pore opening. Despite this, it can be seen that the pore opening in MOF-801 is not dominated from this particular region. This is in contrast with d-MOF-801(35) and d-MOF-801(50) where their pore width is dominated at the region around 1.2 nm. The pore opening within this region could then be considered optimal for diclofenac adsorption because of the molecular size of diclofenac molecule (0.52 × 0.74 × 1.03 nm) [39].

3.2. Diclofenac adsorption performance of MOF-801 and d-MOF-801(n)

3.2.1. Diclofenac adsorption kinetic and isotherm

Having fully characterised the MOF-801 and d-MOF-801(n), we then continue to study their diclofenac adsorption performance. Diclofenac is chosen because it is one of the most popular NSAIDs that has been used worldwide. However, its immediate release to the environment should be avoided since its accumulation could harm the surrounding environment. With the aid of defect engineering in MOF-801, the adsorption performance of this particular MOF can be expected to be enhanced.

First, the kinetic study of both d-MOF-801(n) and MOF-801 were conducted and the result is presented in Fig. 5 with the value of their parameters is shown in Table 3. It can be firstly observed that both d-MOF-801(n) and MOF-801 could reach the adsorption equilibrium in less than 1 h. This time to reach equilibrium is considerably fast, when it is compared with, for example, MIL-100 [39]. Although the maximum adsorption capacity of MIL-100 is higher than d-MOF-801(n), it requires more than 20 h for the adsorption to reach equilibrium. This could then be attributed to the pore opening around 1.2 nm that could avoid the diffusion resistance for the diclofenac to get adsorbed onto the active sites of d-MOF-801(n).

Based on the further analysis, the kinetic model of both d-MOF-801 (n) and MOF-801 suits better with the pseudo-second order (PSO) kinetic model fits better in comparison to the pseudo-first order (PFO). Although the fitting is based on the linearised model, it can also be seen from Table S2 that an agreement can also be obtained when the data is

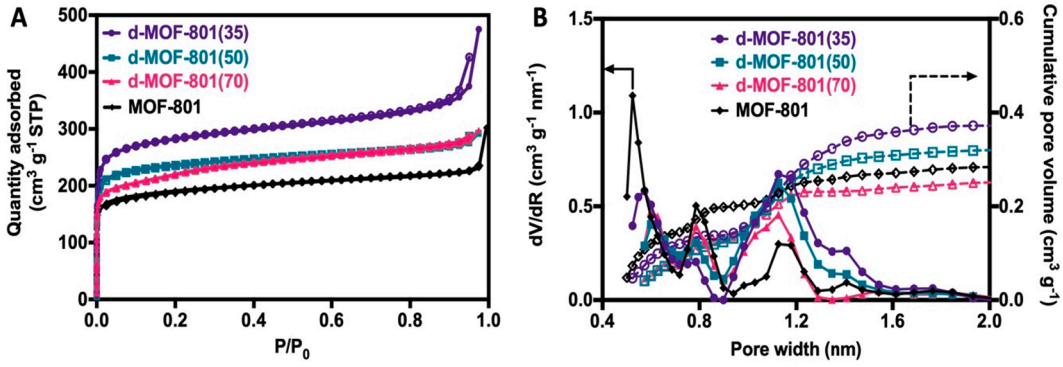

Fig. 4. The nitrogen adsorption at 77 K (A) and the pore width distribution and cumulative pore volume (B) of MOF-801 and d-MOF-801(n).

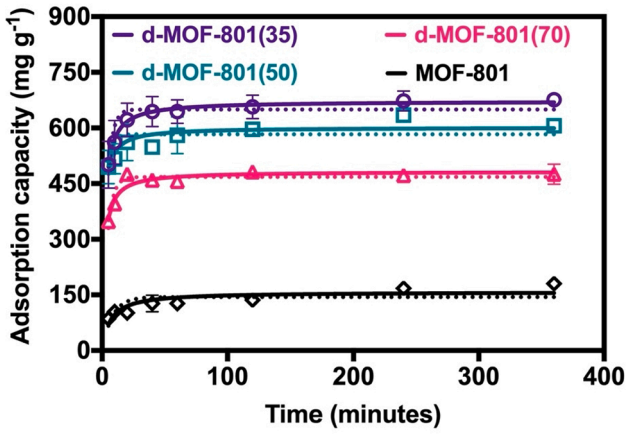

Fig. 5. The diclofenac adsorption kinetics of d-MOF-801(n) and MOF-801. The PSO and PFO fitting are shown as solid and dotted line, respectively.

Table 3
The value of parameters in PFO and PSO model.

Parameter	d-MOF-801 (35)	d-MOF-801 (50)	d-MOF-801 (70)	MOF-801
PFO				
q_{eq}	106.5	157.4	33	94.8
k_1	0.0081	0.0169	0.0104	0.0064
R^2	0.74	0.94	0.27	0.95
PSO				
q_{eq}	657.9	588.2	454.5	156.3
k_2	0.000582	0.000672	0.001466	0.000246
R^2	0.999	0.998	0.999	0.985

fitted using non-linearised model, where PSO fits better than the PFO model to describe the kinetic process of diclofenac adsorption. Based on the PSO model, the equilibrium adsorption capacity for the MOF-801 is then found to be around 156 mg g^{-1}. This is in contrast with the equilibrium adsorption capacity found in d-MOF-801(n). In this case, the equilibrium capacity for d-MOF-801(35), d-MOF-801(50) and d-MOF-801(70) are found to be around 657, 588 and 454 mg g^{-1}, respectively.

To gain further insight on the diclofenac adsorption phenomena in the MOF-801 and d-MOF-801(n), intraparticle diffusion (IPD) model is also used to analyse the kinetic data of the diclofenac adsorption. The result for the analysis is presented in Fig. 6(A) and Table S3. From the results it can be seen that there are two distinct trends, each is owned by MOF-801 and d-MOF-801(n). For MOF-801, the IPD model can be well fitted with a one-step linear trend. However, this one-step process cannot be applied for d-MOF-801(n). From the results, all d-MOF-801(n) shows two linear steps in the IPD model. During the adsorption process, three important diffusional steps could be involved: (i) the diffusion of the adsorbate from the film layer to the particle, (ii) adsorbate diffusion in the pores of the particles and (iii) surface diffusion of the adsorbate before being adsorbed [40]. One of these diffusional processes could then act as the rate limiting step during the adsorption process. In the presence of multilinearity, the whole adsorption mechanism in d-MOF-801(n) is probably not governed by the diffusion of the adsorbate in the pores of the MOF. In contrast, the linearity exhibited by the MOF-801 might indicate that the adsorbate diffusion in the pores of MOF-801 (pore diffusion) might be the limiting step during the adsorption process [41].

This is the further corroborated by analysing further the kinetic data using the Boyd model and the result is presented in Fig. 6(B) and Table S4. As in IPD model, it can also be seen from the Boyd model that there are two distinct trends, each is owned by MOF-801 and d-MOF-801 (n). MOF-801 exhibits a linear trend while all d-MOF-801(n) shows a multilinear trend. In addition, it can also be observed that the linear trend of MOF-801 passes the origin. In Boyd model, when the linear trend does not pass the origin, it indicates that the kinetic of the adsorption process is not governed by intraparticle diffusion [42]. In the case of MOF-801, this then means that the diffusion from the film to the particles are fast and the adsorption process is governed by the diffusion of the adsorbate in the pores of the particles. This is actually understandable since the continuous agitation during the experiment could eliminate the film diffusion [43] and thus the adsorption kinetic of diclofenac onto the MOF-801 is more governed by the adsorbate diffusion in the MOF-801 itself.

In contrast, the multilinearity of d-MOF-801(n) might indicate that neither the adsorbate diffusion in the film to the particle nor the adsorbate diffusion in the pore of the MOFs governs the overall kinetic in the d-MOF-801(n). This could be expected since the pore enlargement in all d-MOF-801(n), which is induced by the presence of defects, might contribute in enhancing the diffusional process of the diclofenac during the adsorption process. As a result, this pore diffusion might no longer act as the rate-limiting step as observed in MOF-801. Therefore, in this case, it could be the case that the surface diffusion of diclofenac before adsorption on the surface of d-MOF-801(n) might govern the overall kinetic process.

The diclofenac adsorption isotherm of MOF-801 and d-MOF-801(n) was also then studied and the result is presented in Fig. 7 with the values of their parameters based on the linearised Langmuir and Freundlich models are given in Table 4. As can be seen, the MOF-801 has the lowest diclofenac adsorption capacity compared with the d-MOF-801(n). Based on the Langmuir model, the maximum adsorption capacity of MOF-801 is found to be around 173 mg g^{-1}, which agrees with the estimated equilibrium adsorption capacity from the kinetic study. The diclofenac maximum adsorption capacity of MOF-801 is also comparable with the diclofenac adsorption capacity in UiO-66, which falls around 100 mg g^{-1} [24]. This result is expected since both materials share the structural similarity. The slightly higher capacity observed in MOF-801

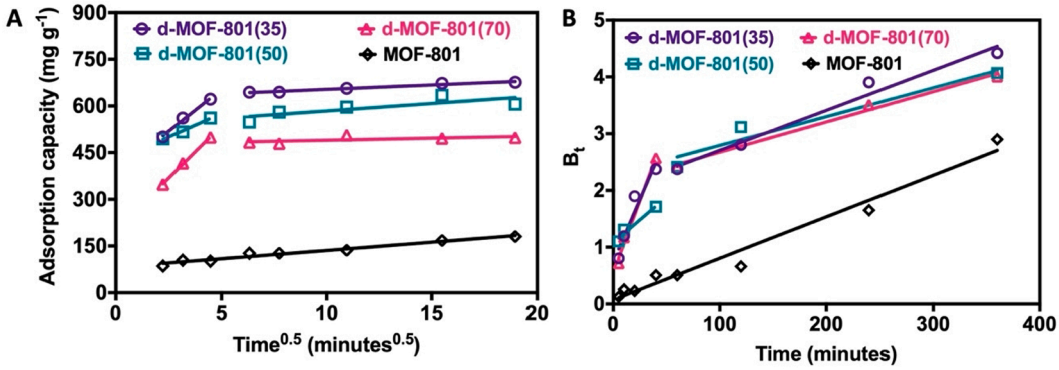

Fig. 6. The intraparticle diffusion (IPD) (A) and Boyd (B)model of d-MOF-801(n) and MOF-801 for diclofenac adsorption.

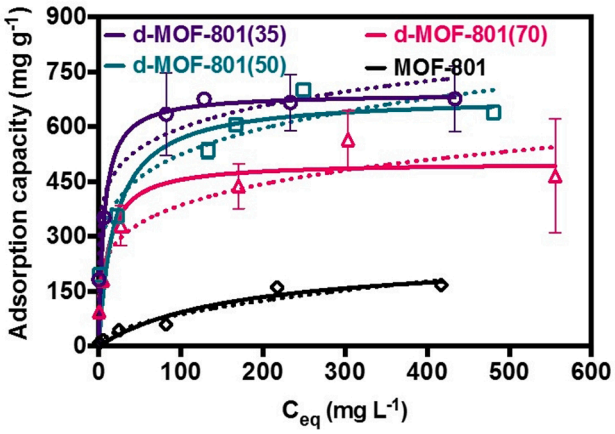

Fig. 7. The diclofenac adsorption isotherms of d-MOF-801(n) and MOF-801. The Langmuir and Freundlich fitting are shown as solid and dotted line, respectively.

Table 4
The value of parameters in Langmuir and Freundlich model.

Parameter	d-MOF-801 (35)	d-MOF-801 (50)	d-MOF-801 (70)	MOF-801
Langmuir model				
q_{max}	680	667	485	173
K_L	0.154	0.082	0.265	0.052
R^2	0.999	0.991	0.988	0.99
Freundlich model				
K_f	273.6	188.3	141.7	12.6
n	0.163	0.217	0.217	0.408
R^2	0.914	0.883	0.895	0.732

could then be associated with the presence of a little number of defects in this particular sample. As has been previously explained, our attempt to synthesise a perfect MOF-801 was proven unsuccessful since the formate group was always present. From the pore size distribution analysis of MOF-801, it can also be seen that the pore at around 1 nm do still exist, albeit it is not the dominant constituent. The presence of these little defects in the MOF-801 might then aid in enhancing its diclofenac adsorption compared with the UiO-66 since the size of the diclofenac molecule might fit well to go into the MOF-801.

In contrast, all the d-MOF-801(n) show higher diclofenac adsorption capacity compared with its MOF-801 counterpart. From the Langmuir model, it can be predicted that the maximum adsorption capacity of the d-MOF-801(35), d-MOF-801(50) and d-MOF-801(70) are found to be around 680, 667 and 425 mg g^{-1}, respectively. This then agrees with the equilibrium adsorption capacity found during the kinetic study and also with the non-linearised Langmuir model (Table S5). Therefore, it could be concluded that the lower the formic acid used to synthesise d-MOF-801(n), the higher its maximum diclofenac adsorption capacity. This trend can then be associated with the increasing number of defects in the d-MOF-801(n) when it was synthesised with lower amount of formic acid. This result also corroborates previous characterisations that show that among the d-MOF-801 samples, d-MOF-801(35) has the highest surface area with pore opening dominated at around 1.2 nm and thus more effective in capturing diclofenac molecules. This then highlights the importance of having a more porous structure in d-MOF-801(n) in capturing diclofenac from water streams.

3.2.2. The effects of temperature, pH and salts on the diclofenac adsorption performance

The effect of temperature on the diclofenac adsorption on both MOF-801 and d-MOF-801(35) is also evaluated with the result is given in Fig. 8(A). From the result, it can be seen that the adsorption capacity of both MOF decreases with the increase of temperature. The change in enthalpy value as tabulated in Table S4 is found to be around −5.7 and −9.4 kJ mol^{-1} for MOF-801 and d-MOF-801(35), respectively. This shows the exothermic nature of the diclofenac adsorption in both MOFs, which is also previously observed in other MOFs [44,19]. The diclofenac adsorption process is then more favourable to occur at lower temperature. Higher temperature might increase the solubility of diclofenac in water and thus reducing its possibility to get adsorbed on the MOF surface. Further thermodynamic analysis is then carried out and the result is also tabulated in Table S4. From the result, it can be seen that both MOFs exhibit negative change in entropy (ΔS) during the adsorption process. This indicates the reduction of randomness degree of the

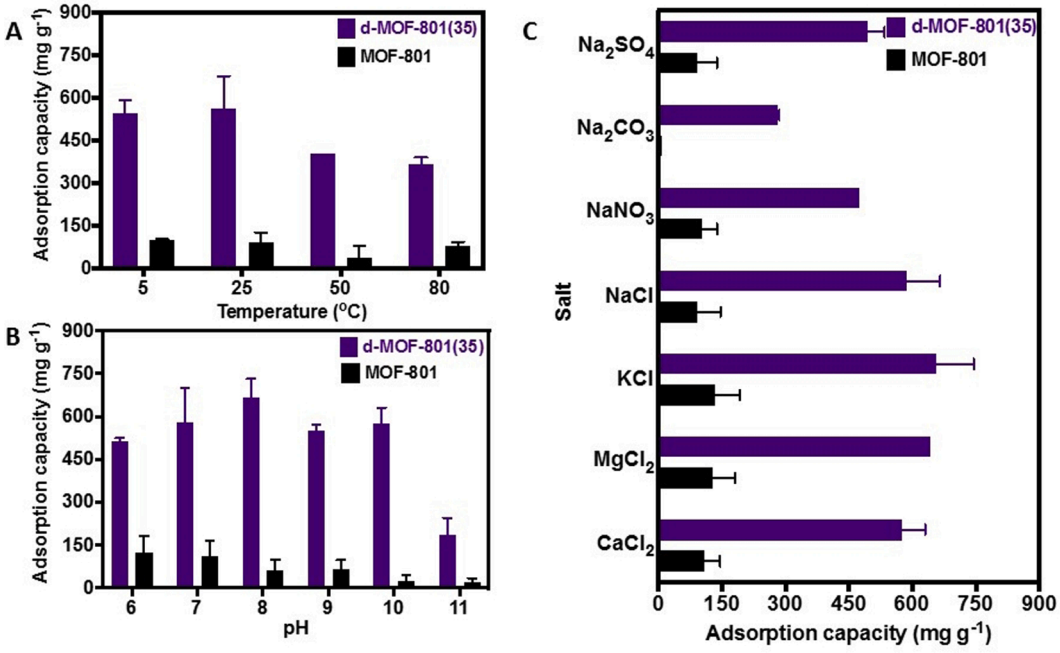

Fig. 8. The effect of temperature (A), pH (B) and the presence of various salts (C) on the diclofenac adsorption performance of d-MOF-801(35) and MOF-801.

diclofenac molecule as it is adsorbed on the surface of either MOF-801 or dMOF-801(35) [45]. As with the change in entropy, the change in Gibbs energy (ΔG) for d-MOF-801(35) is also negative and thus indicates the spontaneity of the diclofenac adsorption process on the surface of d-MOF-801(35). In contrast, the ΔG value in MOF-801 is always positive across the temperature used in this study. The trend is also increasing as the temperature is elevated. A similar behaviour was also previously observed in the adsorption of diclofenac on biochars [46]. This then indicates the existence of energy barrier between the diclofenac and MOF-801 that hinders the spontaneous adsorption process of diclofenac onto the active sites of MOF-801. Therefore, it could be safely concluded that the diclofenac adsorption process in d-MOF-801(35) occurs in a more spontaneous and favourable way than in MOF-801, which might be attributed to the presence of the defects in the d-MOF-801(35).

The effect of pH on the adsorption capacity of both MOF-801 and d-MOF-801(35) was also evaluated. From the result in Fig. 8(B), it can be seen that change in pH between 6 and 10 does not significantly alter the adsorption capacity in d-MOF-801(35). The adsorption capacity for d-MOF-801(35) can still be maintained around 600 mg g^{-1}. In contrast, the adsorption capacity for MOF-801 is observed to be declining starting at around pH 8. At this pH, the adsorption capacity of MOF-801 is found to be around 64 mg g^{-1}, which is less than half of its maximum capacity. This capacity then further declines to be around 20 mg g^{-1} when the pH is further increased to 11. Meanwhile, although also experiencing a decline, d-MOF-801(35) can still retain about 30% of its maximum adsorption capacity, which is around 187 mg g^{-1}, at pH 11. The influence of high pH in diminishing the adsorbent capability to remove diclofenac has also been previously investigated [19,47,48]. The declining capacity of the diclofenac adsorption capacity in d-MOF-801 (35) could then be explained by the competitive adsorption from the anion in the solution. In this case, diclofenac molecules have to compete with the OH^- to get adsorbed on the surface of d-MOF-801(35).

In addition to temperature and pH, the adsorption capacity of a porous material can also be affected by the presence of various salts. This was then also investigated with the result is presented in Fig. 8(C). As can be seen, in general, the presence of various salts in the solution does not significantly alter the adsorption capacity of both MOF-801 and d-MOF-801(35), in particular in the presence of various chloride salts (NaCl, KCl, $MgCl_2$ and $CaCl_2$). The adsorption capacity of both materials can still be maintained around 130 and 650 mg g^{-1}, respectively. Therefore, in these cases, the presence of cations and anions from the salts might not compete with the diclofenac anion to get adsorbed either on d-MOF-801(35) or MOF-801. In contrast, a decrease in adsorption capacity in the presence of various natrium salts such as $NaNO_3$, Na_2SO_4 and Na_2CO_3 could be observed. As can be seen, a decrease around 10–20% from the maximum adsorption capacity can be observed for both MOF-801 and d-MOF-801(35) in the presence of these salts. This might then be attributed to the competitive adsorption between the anion species from the salt and diclofenac resulting in the lower adsorption capacity for the latter on the MOF [15]. Moreover, this effect could be more pronounced in the presence of divalent anion since they could establish stronger interaction with the MOF and thus inducing a more competitive environment for the adsorption of diclofenac molecule. In the case of Na_2CO_3, the salt is also responsible in increasing the pH of the solution and thus, as previously discussed, will also result in the reduction of diclofenac adsorption capacity.

The excellent performance of d-MOF-801 for diclofenac removal in comparison with MOF-801 could then be attributed to several factors. Firstly, as has been explained, the presence of defects in the d-MOF-801 could contribute in opening the pores in d-MOF-801 and thus resulting in better access of diclofenac to the adsorption sites on d-MOF-801. This is then corroborated by the significant reduction of the nitrogen uptake of d-MOF-801(35) after diclofenac adsorption (Figure S5). This then indicates that the majority of the surface area in d-MOF-801(35) has now been occupied by diclofenac molecule. When this defect does not exist or its presence is very minimal, as in the case in MOF-801, the existing pore window is not large enough to let diclofenac molecule to pass through the pore and access the adsorption active sites. This hypothesis is also backed by observing the FTIR spectra after diclofenac adsorption both on d-MOF-801(35) and MOF-801 as given in Figure S6. From the figure, it can be clearly seen that numerous peaks belonging to diclofenac appear in the d-MOF-801(35) after the adsorption process. In contrast, such peaks can be barely seen in MOF-801 and thus indicating the minimal presence of diclofenac in the pores of MOF-801.

Secondly, this could also be attributed to the zeta potential of the d-MOF-801. In this case, the introduction of defective sites in MOF-801 does seem to significantly alter the trend of zeta potential in the MOF. As can be seen in Figure S7, the zeta potential of d-MOF-801(35) is highly positive, even at a high pH. This is in contrast with the MOF-801, that has negative zeta potential at pH above 7. As a result, an electrostatic attraction between the diclofenac anion and the surface of d-MOF-801(35) could be very well established. In contrast, the electrostatic repulsion between MOF-801 and diclofenac anion might be also responsible in establishing the energy barrier that hinders the spontaneity of the adsorption process [46]. The highly positive zeta potential exhibited by d-MOF-801(35) could then also contribute in the establishment of cation-π interaction between the d-MOF-801(35) and the electron-rich benzene ring of the diclofenac molecule, which could eventually enhance its adsorption performance. All of these factors might then play a significant role in enhancing the diclofenac adsorption capacity of the d-MOF-801.

Fig. 9 then depicts the adsorption mechanism comparison between MOF-801 and d-MOF-801. As can be seen, the effective removal of diclofenac molecule from water in d-MOF-801(n) is mostly attributed to the presence of defective sites that allow the diclofenac molecule to go inside the pore of d-MOF-801. Once inside, various interactions such as electrostatic and cation-π interactions could then be established between the active sites of d-MOF-801(n) and diclofenac molecule. This is in contrast with MOF-801 where the diclofenac molecule does not have access to these adsorption sites and thus could only sit on the outer surface of the MOF. As a consequence, MOF-801 is highly ineffective to remove diclofenac from the water stream.

3.2.3. Adsorbent regeneration and diclofenac adsorption performance comparison with other adsorbents

As d-MOF-801(35) shows the most promising performance, the ability of the material to be regenerated was also evaluated to prove its efficacy to undergo multiple adsorption cycles. As can be seen in Fig. 10 (A), after solvent washing, the diclofenac adsorption capacity of d-MOF-801(35) can be retained for at least 4 adsorption cycles. The slight increase of the adsorption capacity in the second and third cycle could then be attributed to various factors such as the elimination of some guest molecules inside the pores which had not been successfully removed before the first cycle took place. Overall, the adsorption capacity of d-MOF-801(35) can be maintained at around 600 mg g^{-1} during the 4 cycles of adsorption test (3 regeneration cycles), although a slight decrease was observed in the last cycle which might be caused by various factors such as structural degradations or the adsorbents exhaustion. The satisfactory adsorption performance maintenance of d-MOF-801(35) is also confirmed through PXRD characterization. From Fig. 10(B), it can be seen that the crystallinity of the d-MOF-801(35) is also maintained after undergoing multiple adsorption cycles. This then indicates that, despite the high defect concentration in d-MOF-801(35), the inherent nature of robust structure owned in MOF-801 structure can still be well-retained in d-MOF-801(35) and thus contributing in excellent performance to be applied for multiple adsorption cycles.

Lastly, to give a broader perspective regarding the performance of d-MOF-801(n) for diclofenac adsorption, Table 5 gives a comparison performance across various porous materials that have been studied for diclofenac removal. From the result, it can be seen that the performance of d-MOF-801(n) surpasses most of the porous materials that have been recently studied for diclofenac removal. In particular, d-MOF-801(n) can

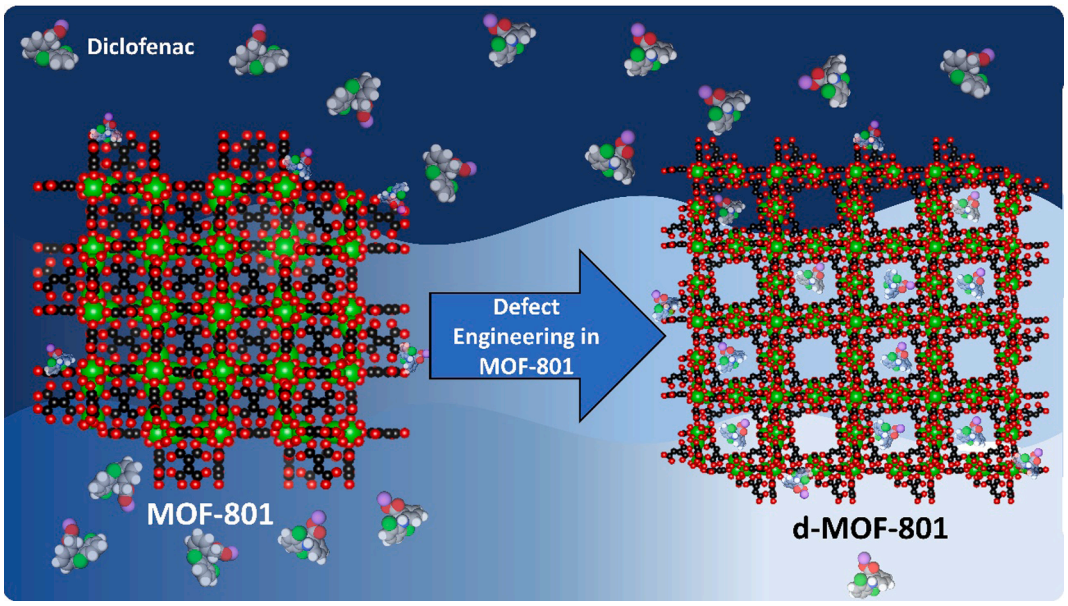

Fig. 9. Comparison of diclofenac adsorption from water stream in MOF-801 and d-MOF-801(n).

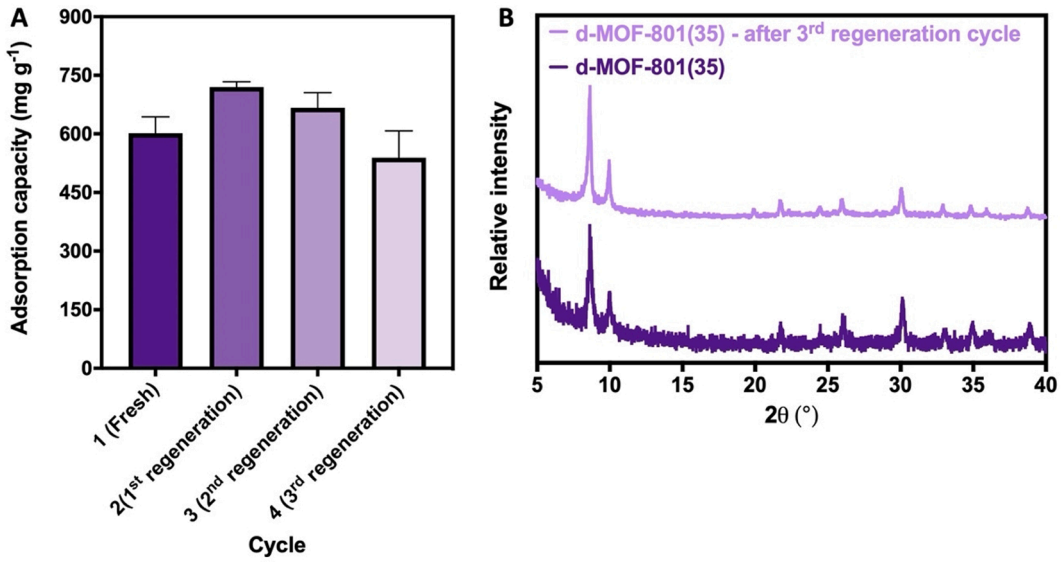

Fig. 10. The diclofenac adsorption performance of d-MOF-801(35) during adsorption–desorption cycling test (A) and its corresponding PXRD pattern (B).

outperform activated carbon, which is the most commercially available porous materials to date. Some of the reported MOFs exhibit higher diclofenac adsorption capacity in comparison with d-MOF-801, for example UiO-66-$(COOFe)_2$ [25]. However, it should be noted that the high performance of this MOF could only be acquired after undergoing a post-synthetic modification process, which also complicates the whole process of adsorbent synthesis. Meanwhile, in the case of d-MOF-801, such a post-synthetic modification process is not required and could even be replaced with the use of benign synthesis condition and the possibility to control the particle size. Together with the adsorption reusability, it can then be expected that d-MOF-801(n) can take over activated carbon to be deployed for this particular application.

4. Conclusions

In this study, we have successfully shown that the defect engineering strategy can be used to enhance diclofenac adsorption capacity of MOF-801. The adsorption capacity of the defect engineered MOF-801 can be increased almost 4 times compared to its MOF-801 counterpart, reaching around 680 mg g^{-1} of maximum diclofenac adsorption capacity. The enhancement of the diclofenac adsorption capacity is achieved by changing the synthesis condition and thus avoiding the complexity of post-synthesis modification, which is usually applied in various adsorbents. The defect concentration in the MOF-801 can be tuned by adjusting the amount of the modulator added during the synthesis. In addition, the defective MOF-801 (i.e. d-MOF-801(35)) can be recycled (up to 4 times) with only a slight compromise on its diclofenac adsorption performance. Together with a relatively benign and simple synthesis condition, the developed defective MOF-801 has shown to be a promising adsorbent material for removal of diclofenac from water streams.

Table 5
The comparison of diclofenac adsorption performance from various porous materials.

Porous materials	Maximum diclofenac adsorption capacity (mg g^{-1})*	Reference
Activated carbon from sewage sludge	84–155	[49]
Activated carbon from olive stones	11	[5]
Functionalised activated carbon	490	[3]
Chemically and thermally treated soybean hull	122–136	[50]
Organoclays	36–172	[6]
Graphene oxide	500	[9]
Maghemite	120–252	[51]
Composite gelatin / carbon nanotube	27	[13]
Zn-Al LDH.xBi_2O_3	574	[12]
Amino-functionalised cellulose nanocrystals / chitosan	444	[11]
Magnetic COF (TPB-DMTP)	71	[52]
UiO-66	189	[23]
18% SO_3H-UiO-66	263	
UiO-66-$(COOCu)_2$	624	[25]
UiO-66-$(COOFe)_2$	796	
Fe_3O_4@MOF-100 (Fe)	298–438	[53]
Fe_3O_4-FeBTC	347	[44]
NH_2-UiO-66	357–555	[24]
MIL-100	773	[39]
MOF-808	833	[19]
MOF-801	174	This study
d-MOF-801(35)	680	
d-MOF-801(50)	667	
d-MOF-801(70)	485	

* Unless otherwise stated, the value is estimated from Langmuir isotherm.

CRediT authorship contribution statement

Nicholaus Prasetya: Conceptualization, Methodology, Software, Validation, Formal analysis, Investigation, Data curation, Writing – original draft, Writing – review & editing, Visualization. **Kang Li:** Conceptualization, Methodology, Resources, Writing – review & editing, Supervision, Project administration, Funding acquisition.

Declaration of Competing Interest

The authors declare that they have no known competing financial interests or personal relationships that could have appeared to influence the work reported in this paper.

Data availability

Data will be made available on request.

Acknowledgments

The authors gratefully acknowledge the Engineering and Physical Science Research Council Funding (Grant Number EP/J014974/1)

Appendix A. Supplementary material

Supplementary data to this article can be found online at https://doi.org/10.1016/j.seppur.2022.122024.

References

[1] L. Lonappan, S.K. Brar, R.K. Das, M. Verma, R.Y. Surampalli, Diclofenac and its transformation products: environmental occurrence and toxicity-a review, Environ. Int. 96 (2016) 127–138.
[2] L. Lonappan, T. Rouissi, S.K. Brar, M. Verma, R.Y. Surampalli, Adsorption of diclofenac onto different biochar microparticles: dataset–characterization and dosage of biochar, Data Brief 16 (2018) 460–465.
[3] B.N. Bhadra, P.W. Seo, S.H. Jhung, Adsorption of diclofenac sodium from water using oxidized activated carbon, Chem. Eng. J. 301 (2016) 27–34.
[4] M.D.G. de Luna, Murniati, W. Budianta, K.K.P. Rivera, R.O. Arazo, Removal of sodium diclofenac from aqueous solution by adsorbents derived from cocoa pod husks, J. Environ. Chem. Eng. 5 (2) (2017) 1465–1474.
[5] S. Larous, A.-H. Meniai, Adsorption of Diclofenac from aqueous solution using activated carbon prepared from olive stones, Int. J. Hydrog. Energy 41 (24) (2016) 10380–10390.
[6] T. De Oliveira, R. Guégan, T. Thiebault, C. Le Milbeau, F. Muller, V. Teixeira, M. Giovanela, M. Boussafir, Adsorption of diclofenac onto organoclays: Effects of surfactant and environmental (pH and temperature) conditions, J. Hazard. Mater. 323 (2017) 558–566.
[7] J.J.M. Garcia, J.A.P. Nuñez, H.S. Salapare, M.R. Vasquez, Adsorption of diclofenac sodium in aqueous solution using plasma-activated natural zeolites, Results Phys. 15 (2019), 102629.
[8] A.C.S. Guerra, M.B. de Andrade, T.R. Tonial dos Santos, R. Bergamasco, Adsorption of sodium diclofenac in aqueous medium using graphene oxide nanosheets, Environ. Technol. 42 (16) (2021) 2599–2609.
[9] S.-W. Nam, C. Jung, H. Li, M. Yu, J.R. Flora, L.K. Boateng, N. Her, K.-D. Zoh, Y. Yoon, Adsorption characteristics of diclofenac and sulfamethoxazole to graphene oxide in aqueous solution, Chemosphere 136 (2015) 20–26.
[10] C.B. Godiya, S. Kumar, Y. Xiao, Amine functionalized egg albumin hydrogel with enhanced adsorption potential for diclofenac sodium in water, J. Hazard. Mater. 393 (2020), 122417.
[11] D. Hu, H. huang, R. Jiang, N. Wang, H. Xu, Y.-G. Wang, X.-K. Ouyang, Adsorption of diclofenac sodium on bilayer amino-functionalized cellulose nanocrystals/chitosan composite, J. Hazard. Mater. 369 (2019) 483–493.
[12] P. Kumari, B. Pal, R.K. Das, Superior adsorptive removal of eco-toxic drug diclofenac sodium by Zn–Al LDH· xBi2O3 layer double hydroxide composites, Appl. Clay Sci. 208 (2021), 106119.
[13] C.V.T. Rigueto, M. Rosseto, M.T. Nazari, B.E.P. Ostwald, I. Alessandretti, C. Manera, J.S. Piccin, A. Dettmer, Adsorption of diclofenac sodium by composite beads prepared from tannery wastes-derived gelatin and carbon nanotubes, J. Environ. Chem. Eng. 9 (1) (2021), 105030.
[14] D. Smiljanić, B. de Gennaro, F. Izzo, A. Langella, A. Daković, C. Germinario, G. E. Rottinghaus, M. Spasojević, M. Mercurio, Removal of emerging contaminants from water by zeolite-rich composites: A first approach aiming at diclofenac and ketoprofen, Microporous Mesoporous Mater. 298 (2020), 110057.
[15] T. Xiong, X. Yuan, H. Wang, Z. Wu, L. Jiang, L. Leng, K. Xi, X. Cao, G. Zeng, Highly efficient removal of diclofenac sodium from medical wastewater by Mg/Al layered double hydroxide-poly (m-phenylenediamine) composite, Chem. Eng. J. 366 (2019) 83–91.
[16] K.-Y.-A. Lin, Y.-T. Liu, S.-Y. Chen, Adsorption of fluoride to UiO-66-NH2 in water: stability, kinetic, isotherm and thermodynamic studies, J. Colloid Interface Sci. 461 (2016) 79–87.
[17] X. Liu, N.K. Demir, Z. Wu, K. Li, Highly water-stable zirconium metal–organic framework UiO-66 membranes supported on alumina hollow fibers for desalination, J. Am. Chem. Soc. 137 (22) (2015) 6999–7002.
[18] M. Massoudinejad, M. Ghaderpoori, A. Shahsavani, M.M. Amini, Adsorption of fluoride over a metal organic framework Uio-66 functionalized with amine groups and optimization with response surface methodology, J. Mol. Liq. 221 (2016) 279–286.
[19] N. Prasetya, K. Li, MOF-808 and its hollow fibre adsorbents for efficient diclofenac removal, Chem. Eng. J. 417 (2021), 129216, https://doi.org/10.1016/j.cej.2021.129216.
[20] G. Wißmann, A. Schaate, S. Lilienthal, I. Bremer, A.M. Schneider, P. Behrens, Modulated synthesis of Zr-fumarate MOF, Microporous Mesoporous Mater. 152 (2012) 64–70.
[21] H. Kim, S.R. Rao, E.A. Kapustin, L. Zhao, S. Yang, O.M. Yaghi, E.N. Wang, Adsorption-based atmospheric water harvesting device for arid climates, Nat. Commun. 9 (2018) 1–8.
[22] K.H. Cho, P.G.M. Mileo, J.S. Lee, U.-H. Lee, J. Park, S.J. Cho, S.K. Chitale, G. Maurin, J.-S. Chang, Defective Zr-fumarate MOFs enable high-efficiency adsorption heat allocations, ACS Appl. Mater. Interfaces 13 (1) (2021) 1723–1734.
[23] Z. Hasan, N.A. Khan, S.H. Jhung, Adsorptive removal of diclofenac sodium from water with Zr-based metal–organic frameworks, Chem. Eng. J. 284 (2016) 1406–1413.
[24] S. Zhuang, R. Cheng, J. Wang, Adsorption of diclofenac from aqueous solution using UiO-66-type metal-organic frameworks, Chem. Eng. J. 359 (2019) 354–362.
[25] H.A. Younes, M. Taha, R. Mahmoud, H.M. Mahmoud, R.M. Abdelhameed, High adsorption of sodium diclofenac on post-synthetic modified zirconium-based metal-organic frameworks: experimental and theoretical studies, J. Colloid Interface Sci. 607 (2022) 334–346.
[26] R. Hardian, S. Dissegna, A. Ullrich, P.L. Llewellyn, M.-V. Coulet, R.A. Fischer, Tuning the properties of MOF-808 via defect engineering and metal nanoparticle encapsulation, Chem. Eur. J. 27 (22) (2021) 6804–6814.
[27] Villajos, J.A., Jagorel, N., Reinsch, S., Emmerling, F., 2019. Increasing exposed metal site accessibility in a Co-MOF-74 material with induced structure-defects. Front. Mater. 230.
[28] C.A. Clark, K.N. Heck, C.D. Powell, M.S. Wong, Highly defective UiO-66 materials for the adsorptive removal of perfluorooctanesulfonate, ACS Sustain. Chem. Eng. 7 (7) (2019) 6619–6628.

[29] Y.i. Feng, Q. Chen, M. Jiang, J. Yao, Tailoring the properties of UiO-66 through defect engineering: a review, Ind. Eng. Chem. Res. 58 (38) (2019) 17646–17659.
[30] P. Iacomi, F. Formalik, J. Marreiros, J. Shang, J. Rogacka, A. Mohmeyer, P. Behrens, R. Ameloot, B. Kuchta, P.L. Llewellyn, Role of structural defects in the adsorption and separation of C3 hydrocarbons in Zr-fumarate-MOF (MOF-801), Chem. Mater. 31 (20) (2019) 8413–8423.
[31] P.G.M. Mileo, K.H. Cho, J.-S. Chang, G. Maurin, Water adsorption fingerprinting of structural defects/capping functions in Zr–fumarate MOFs: a hybrid computational-experimental approach, Dalton Trans. 50 (4) (2021) 1324–1333.
[32] J. Ren, M. Ledwaba, N.M. Musyoka, H.W. Langmi, M. Mathe, S. Liao, W. Pang, Structural defects in metal–organic frameworks (MOFs): formation, detection and control towards practices of interests, Coord. Chem. Rev. 349 (2017) 169–197.
[33] K.I. Hadjiivanov, D.A. Panayotov, M.Y. Mihaylov, E.Z. Ivanova, K.K. Chakarova, S. M. Andonova, N.L. Drenchev, Power of infrared and raman spectroscopies to characterize metal-organic frameworks and investigate their interaction with guest molecules, Chem. Rev. 121 (2021) 1286–1424, https://doi.org/10.1021/acs.chemrev.0c00487.
[34] G. Zahn, H.A. Schulze, J. Lippke, S. König, U. Sazama, M. Fröba, P. Behrens, A water-born Zr-based porous coordination polymer: Modulated synthesis of Zr-fumarate MOF, Microporous Mesoporous Mater. 203 (2015) 186–194.
[35] D. Feng, K. Wang, Z. Wei, Y.-P. Chen, C.M. Simon, R.K. Arvapally, R.L. Martin, M. Bosch, T.-F. Liu, S. Fordham, D. Yuan, M.A. Omary, M. Haranczyk, B. Smit, H.-C. Zhou, Kinetically tuned dimensional augmentation as a versatile synthetic route towards robust metal–organic frameworks, Nat. Commun. 5 (1) (2014).
[36] G.C. Shearer, S. Chavan, J. Ethiraj, J.G. Vitillo, S. Svelle, U. Olsbye, C. Lamberti, S. Bordiga, K.P. Lillerud, Tuned to perfection: ironing out the defects in metal–organic framework UiO-66, Chem. Mater. 26 (14) (2014) 4068–4071.
[37] V.V. Butova, I.A. Pankin, O.A. Burachevskaya, K.S. Vetlitsyna-Novikova, A. V. Soldatov, New fast synthesis of MOF-801 for water and hydrogen storage: modulator effect and recycling options, Inorganica Chim. Acta 514 (2021), 120025.
[38] Y. Jiao, Y. Liu, G. Zhu, J.T. Hungerford, S. Bhattacharyya, R.P. Lively, D.S. Sholl, K. S. Walton, Heat-Treatment of Defective UiO-66 from Modulated Synthesis: adsorption and Stability Studies, J. Phys. Chem. C 121 (2017) 23471–23479, https://doi.org/10.1021/acs.jpcc.7b07772.
[39] S. Zhuang, Y. Liu, J. Wang, Mechanistic insight into the adsorption of diclofenac by MIL-100: Experiments and theoretical calculations, Environ. Pollut. 253 (2019) 616–624.
[40] R.M.C. Viegas, M. Campinas, H. Costa, M.J. Rosa, How do the HSDM and Boyd's model compare for estimating intraparticle diffusion coefficients in adsorption processes, Adsorption 20 (5-6) (2014) 737–746.
[41] M.I. El-Khaiary, G.F. Malash, Common data analysis errors in batch adsorption studies, Hydrometallurgy 105 (3-4) (2011) 314–320.
[42] J. Wang, X. Guo, Adsorption kinetic models: Physical meanings, applications, and solving methods, J. Hazard. Mater. 390 (2020), 122156.
[43] O.G. Abatan, P.A. Alaba, B.A. Oni, K. Akpojevwe, V. Efeovbokhan, F. Abnisa, Performance of eggshells powder as an adsorbent for adsorption of hexavalent chromium and cadmium from wastewater, SN Appl. Sci. 2 (2020) 1–13.
[44] A.A. Castañeda Ramírez, E. Rojas García, R. López Medina, J.L. Contreras Larios, R. Suárez Parra, A.M. Maubert Franco, Selective adsorption of aqueous diclofenac sodium, naproxen sodium, and ibuprofen using a Stable Fe3O4–FeBTC Metal-Organic Frameworka, Materials 14 (2021) 2293.
[45] M.S. Shamsudin, S.F. Azha, L. Sellaoui, M. Badawi, A. Bonilla-Petriciolet, S. Ismail, Performance and interactions of diclofenac adsorption using Alginate/Carbon-based Films: experimental investigation and statistical physics modelling, Chem. Eng. J. 428 (2022), 131929.
[46] L. Lonappan, T. Rouissi, S.K. Brar, M. Verma, R.Y. Surampalli, An insight into the adsorption of diclofenac on different biochars: mechanisms, surface chemistry, and thermodynamics, Bioresour. Technol. 249 (2018) 386–394.
[47] X. Ye, Y. Li, H. Lin, Y. Chen, M. Liu, Lignin-based magnetic nanoparticle adsorbent for diclofenac sodium removal: adsorption behavior and mechanisms, J. Polym. Environ. 29 (10) (2021) 3401–3411.
[48] Y. Zhao, F. Liu, X. Qin, Removal of diclofenac from aqueous phase by birnessite: effects of pH and common ions, Water. Air. Soil Pollut. 230 (2019) 1–11.
[49] G.S. dos Reis, M.K. Bin Mahbub, M. Wilhelm, E.C. Lima, C.H. Sampaio, C. Saucier, S.L. Pereira Dias, Activated carbon from sewage sludge for removal of sodium diclofenac and nimesulide from aqueous solutions, Korean J. Chem. Eng. 33 (11) (2016) 3149–3161.
[50] R.M. de Souza, H.B. Quesada, L.F. Cusioli, M.R. Fagundes-Klen, R. Bergamasco, Adsorption of non-steroidal anti-inflammatory drug (NSAID) by agro-industrial by-product with chemical and thermal modification: Adsorption studies and mechanism, Ind. Crops Prod. 161 (2021), 113200.
[51] V.O. Leone, M.C. Pereira, S.F. Aquino, L.C.A. Oliveira, S. Correa, T.C. Ramalho, L. V.A. Gurgel, A.C. Silva, Adsorption of diclofenac on a magnetic adsorbent based on maghemite: experimental and theoretical studies, New J. Chem. 42 (1) (2018) 437–449.
[52] S. Zhuang, R. Chen, Y. Liu, J. Wang, Magnetic COFs for the adsorptive removal of diclofenac and sulfamethazine from aqueous solution: adsorption kinetics, isotherms study and DFT calculation, J. Hazard. Mater. 385 (2020), 121596.
[53] X. Zheng, J. Wang, X. Xue, W. Liu, Y. Kong, R. Cheng, D. Yuan, Facile synthesis of Fe3O4@ MOF-100 (Fe) magnetic microspheres for the adsorption of diclofenac sodium in aqueous solution, Environ. Sci. Pollut. Res. 25 (31) (2018) 31705–31717.